Journal of Power Sources 197 (2012) 310–313

Contents lists available at SciVerse ScienceDirect

Journal of Power Sources

journal homepage: www.elsevier.com/locate/jpowsour

Short communication

Use of B_2O_3 to improve Li^+-ion transport in $LiTi_2(PO_4)_3$-based ceramics

Hongjian Peng[a], Hui Xie[b], John B. Goodenough[b,*]

[a] College of Chemistry and Chemical Engineering, Central South University, Changsha, Hunan 410083, China
[b] Materials Science and Engineering Program, ETC 9.184, University of Texas at Austin, Austin, TX 78712, United States

ARTICLE INFO

Article history:
Received 5 July 2011
Received in revised form
15 September 2011
Accepted 16 September 2011
Available online 21 September 2011

Keywords:
Li^+-ion solid electrolyte
B_2O_3

ABSTRACT

Substitution of B for Ti in $Li_{1+x}Ti_{2-x}B_x(PO_4)_3$ introduces x mobile Li^+ ions per formula unit in the solid-station range $0 < x \leq 0.2$. The B_2O_3 is also an aid to sintering dense ceramics with more uniform particle size. With $x = 0.2$, the room-temperature Li^+-ion conductivity is $\sigma_{Li} = 2.0 \times 10^{-4}$ S cm^{-1} with a motional activation energy of 0.48 eV. For $x > 0.2$, an intergranular B_2O_3-rich second phase impedes intergranular Li^+-ion transport.

© 2011 Elsevier B.V. All rights reserved.

1. Introduction

Lithium-ion batteries are now widely used, but safety and volume energy density remain concerns [1–6]. Replacement of the flammable organic liquid-carbonate electrolyte with a Li^+-ion solid electrolyte, would alleviate safety concerns and increase the volume energy density by eliminating irreversible capacity loss on the initial charge. However, low Li^+-ion conductivity (σ_{Li}) and problems with the interface between a solid electrolyte and solid electrodes, particularly a solid cathode, have prevented realization of competitive all solid-state batteries for most applications [7,8]. On the other hand, use of a solid-electrolyte separator with a liquid electrolyte contacting the cathode would eliminate formation of a passivation layer at the anode while avoiding the difficulties associated with interfacing a solid Li^+-ion electrolyte with a solid insertion-compound cathode.

In this paper, we report the use of a B_2O_3 flux to improve the σ_{Li} of as-sintered $LiTi_2(PO_4)_3$ with the NASICON structure from 10^{-7} S cm^{-1} [9,10] to over 10^{-4} S cm^{-1}. Although Ti(IV) will be reduced on contact with a lithium anode, nevertheless we explored the strategy of using a B_2O_3 flux to improve the interparticle Li^+-ion transport in an oxide Li^+-ion solid electrolyte.

Recently, solid Li^+-ion electrolytes $Li_{1+x}M_xTi_{2-x}(PO_4)_3$ with M = Al or Sc have been reported [11–16] to have a $\sigma_{Li} > 10^{-4}$ S cm^{-1} as a result of increased Li^+-ion concentration in the NASICON framework and of better densification of the phosphate pellets. Here we have increased the densification and the Li^+-ion conduction by using B_2O_3. We determined the solid station range of boron with X-ray diffraction (XRD) and densification with scanning electron microscopy (SEM).

2. Experimental

In a typical synthesis process, Li_2CO_3 (purity: 99.99%), TiO_2(99.9%), $(NH_4)_2HPO_4$ (extra-pure grade) and B_2O_3 (99.9%) were used. The stoichiometric quantities of the components were in the molar ratio of $0.6{:}2{:}3{:}0 \leq x \leq 0.25$. A relatively large amount of excess lithium salt was added to compensate for loss of lithium during the heat treatment. The mixture was ground and reacted in an alumina crucible. The powder was precalcined in air from room temperature to 923 K at 2 K min^{-1}, kept at 923 K for 12 h, and allowed to cool to room temperature in the furnace. The samples were uniaxially pressed into discs 10 mm in diameter in a stainless-steel die at 3 MPa. The pressed discs were sintered from room temperature to 1123 K at 2 K min^{-1}, kept at 1123 K for 4 h, and allowed to cool down in the furnace to room temperature.

Impedance spectroscopy measurements over the frequency range of 1 Hz–1 MHz with a Solarton Impedence Analyzer, model 1287, were made on circa 1-mm-thick pellets having a diameter of 12 mm. Both parallel surfaces of the pellets were sputtered with a layer of gold. A 10 mV voltage was applied over the frequency ranges of the Solarton.

XRD measurements were performed with a Philips PW 1830 diffractometer equipped with a CuK_α source operating at 40 kV and 30 mA. A Rietveld structure refinement was carried out with the Fullprof software package. A Philips SEM was used to obtain images of the pellet morphologies.

* Corresponding author. Tel.: +1 512 293 3635.
E-mail address: jgoodenough@mail.utexas.edu (J.B. Goodenough).

0378-7753/$ – see front matter © 2011 Elsevier B.V. All rights reserved.
doi:10.1016/j.jpowsour.2011.09.046

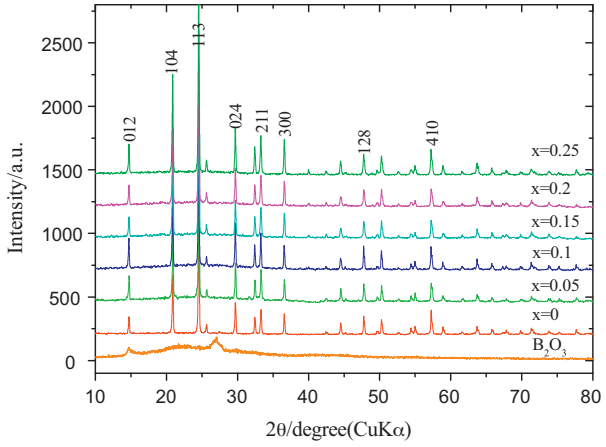

Fig. 1. XRD patterns of $LiTi_2(PO_4)_3$–xB_2O_3 solid state electrolyte and B_2O_3.

Table 1
Lattice parameters and ionic conductivity of $LiTi_2(PO_4)_3$–xB_2O_3 solid state electrolyte.

B_2O_3 (molar fraction)	a (Å)	c (Å)	V (Å)^3	Ionic conductivity (S cm^{-1})
$x=0$	8.509	20.847	1307.2	8.3×10^{-6}
$x=0.05$	8.507	20.844	1306.5	4.5×10^{-5}
$x=0.1$	8.506	20.848	1306.2	5.6×10^{-5}
$x=0.15$	8.506	20.828	1305.5	9.3×10^{-5}
$x=0.2$	8.503	20.832	1304.5	2.0×10^{-4}
$x=0.25$	8.508	20.822	1305.3	1.6×10^{-5}

3. Results

3.1. XRD patterns of $LiTi_2(PO_4)_3$ as a function of B_2O_3 content

Fig. 1 shows XRD patterns of $LiTi_2(PO_4)_3$–xB_2O_3 as a function of B_2O_3 content and B_2O_3. The lattice parameters of pure $LiTi_2(PO_4)_3$–xB_2O_3 are listed in Table 1. As can be seen from the table, the volume decreases with increasing x in the range $0 < x \leq 0.2$, indicating some incorporation of B^{3+} into structure with a compensating increase in the Li^+-ion concentration.

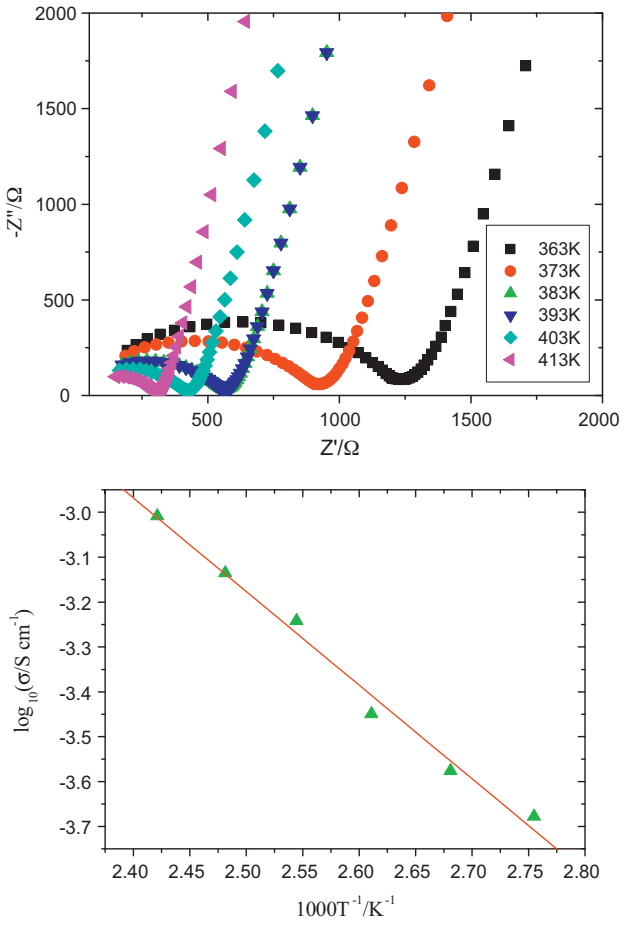

Fig. 3. Temperature dependence of impedance spectroscopy of $LiTi_2(PO_4)_3$–$0.2B_2O_3$.

3.2. Impedance spectroscopy measurements

Fig. 2 shows the room temperature impedance data for $LiTi_2(PO_4)_3$–xB_2O_3 pellets with different values of x. The numerical

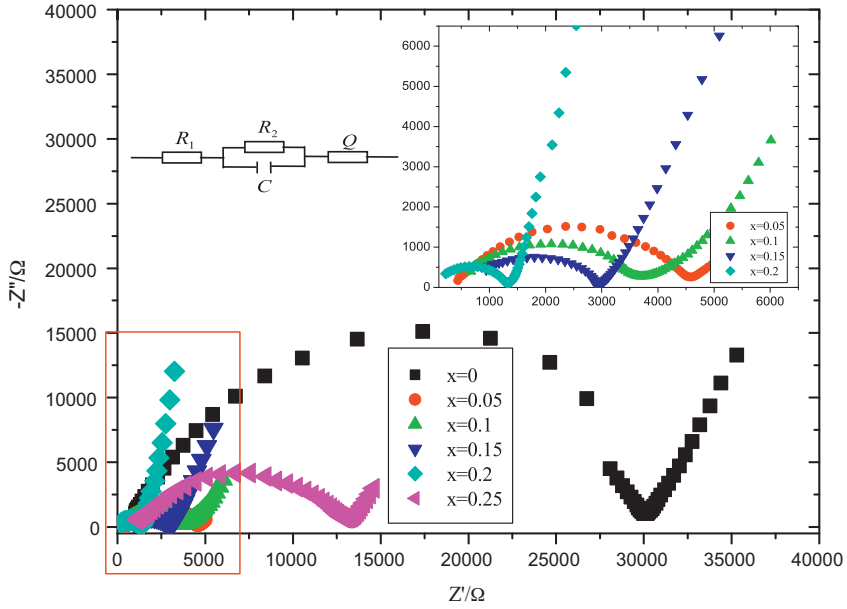

Fig. 2. Impedance spectroscopy of $LiTi_2(PO_4)_3$ as a function of the molar fraction of B_2O_3.

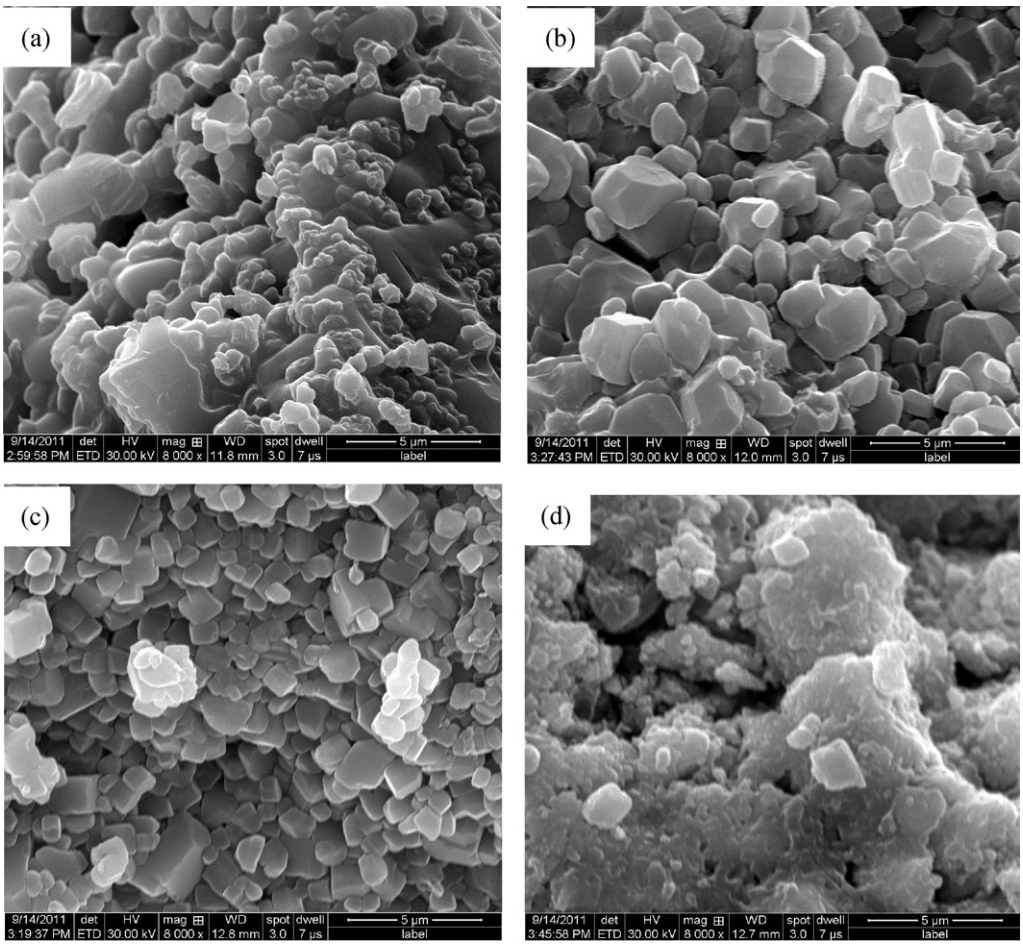

Fig. 4. Cross-sectional SEM images of $LiTi_2(PO_4)_3$–xB_2O_3 as a function of the molar fraction of B_2O_3, $x = 0$ (a), $x = 0.1$ (b), $x = 0.2$ (c), $x = 0.25$ (d).

values for the ionic conductivity at room temperature are listed in Table 1. The inset in Fig. 2 shows the room-temperature impedance data for $LiTi_2(PO_4)_3$–xB_2O_3 pellets from $x = 0.05$ to $x = 0.2$ more clearly. The Li^+-ion conductivity σ_{Li} can be seen to be much higher than that of the pure $LiTi_2(PO_4)_3$, increasing with x to a maximum of 2.0×10^{-4} S cm^{-1} at $x = 0.2$.

3.3. Temperature dependence of impedance spectroscopy of $LiTi_2(PO_4)_3$–$0.2B_2O_3$

The temperature dependence of the impedance spectroscopy of $LiTi_2(PO_4)_3$–$0.2B_2O_3$ from 300 K to 413 K is shown in Fig. 3. From Fig. 3, the Arrhenius plot for $\sigma_{Li} = \sigma_0 \exp(-\varepsilon_a/kT)$, yields an activation energy $\varepsilon_a = 0.48$ eV.

3.4. SEM images of $LiTi_2(PO_4)_3$–xB_2O_3

Fig. 4 shows cross-sectional SEM images, magnified 8000 times, of the evolution of the microstructure of $LiTi_2(PO_4)_3$–xB_2O_3 as a function of B_2O_3 content. $LiTi_2(PO_4)_3$ ($x = 0$) was quite porous with a particle size much larger than that of all the other samples. For $x = 0.2$, the distribution of grain sizes is uniform and the grains are in close contact with each other; pores are few in all the sintered pellets. However Fig. 4(d), shows the presence of a second phase associated with excess B_2O_3. The second phase impedes Li^+-ion transport to lower σ_{Li}.

4. Conclusions

Substitution of B^{3+} ions for Ti^{4+} in $Li_{1+x}Ti_{2-x}B_x(PO_4)_3$, like substitution of Al^{3+} and Sc^{3+}, creates x mobile Li+-ions per formula unit in the interstitial space of the $M_2(PO_4)_3$ framework. The Li^+-ion conductivity increases with x in the solid solution range $0 < x \leq 0.2$ to give, for $x = 0.2$, a room-temperature $\sigma_{Li} = 2 \times 10^{-4}$ S cm^{-1} with a motional activation energy of 0.48 eV. The B_2O_3 also acts as a sintering aid to reduce the grain size while enhancing the intergrain contact. Beyond the solid solution range, a B_2O_3-rich intergranular phase impedes intergranular Li^+-ion transport.

Acknowledgements

I thank the China Scholarship Council for giving me the opportunity to work in Texas. JBG handles the Robert A Foundation of Houston, TX for financial support.

References

[1] Z.H. Chen, Y. Qin, K. Amine, Electrochim. Acta 54 (2009) 5605–5613.
[2] D.Y. Zhou, W.S. Li, C.L. Tan, X.X. Zuo, Y.J. Huang, J. Power Sources 184 (2008) 589–592.
[3] P. Biensan, B. Simon, J.P. Peres, A. de Guibert, M. Broussely, J.M. Bodet, F. Perton, J. Power Sources 82 (1999) 906–912.
[4] C.H. Doh, D.H. Kim, H.S. Kim, H.M. Shin, Y.D. Jeong, S.I. Moon, B.S. Jin, S.W. Eom, K.W. Kim, D.H. Oh, A. Veluchamy, J. Power Sources 175 (2008) 881–885.
[5] E.G. Shim, T.M. Nam, J.G. Kim, H.S. Kim, S.I. Moon, J. Power Sources 175 (2008) 533–539.

[6] Z.-X. Lin, H.-J. Yu, S.-Ch. Li, S.-B. Tian, Solid State Ionics 31 (1988) 91–94.
[7] S. Jacke, J. Song, G. Cherkashinin, L. Dimesso, W. Jaegermann, Chem. Mater. Sci. 16 (2010) 769–775.
[8] M. Landstorfer, S. Funken, T. Jacob, Phys. Chem. Chem. Phys. 13 (2011) 12817–12825.
[9] H. Aono, E. Sugimoto, Y. Sadaoka, N. Imanaka, G. Adachi, J. Electrochem. Soc. 137 (1990) 1023–1027.
[10] H. Aono, E. Sugimoto, Solid State Ionics 47 (1991) 257–264.
[11] K. Arbi, M.G. Lazarraga, D.B. Chehimi, M. Ayadi-Trabelsi, J.M. Rojo, J. Sanz, Chem. Mater. 16 (2004) 255–262.
[12] S. Patous, G. Rousse, J.B. Leriche, C. Masquelier, Chem. Mater. 15 (2003) 2084–2093.
[13] Y.H. Guo, Z. Shi, J.H. Yu, J.D. Wang, Y.L. Liu, N. Bai, W.Q. Pang, Chem. Mater. 13 (2001) 203–207.
[14] Y.H. Guo, Z. Shi, H. Ding, Y.B. Wei, W.Q. Pang, Chin. Chem. Lett. 12 (2001) 373–376.
[15] Y.N. Zhao, G.S. Zhu, X.L. Jiao, W. Liu, W.Q. Pang, J. Mater. Chem. 10 (2000) 463–467.
[16] I. Yu Pinus, I.V. Arkhangel ski, N.A. Zhuravlev, A.B. Yaroslavtsev, Synth. Prop. Inorg. Compd. 8 (2009) 1235–1239.